DepthFocus: Controllable Depth Estimation for See-Through Scenes

Junhong Min^{1,†}, Jimin Kim¹, Cheol-Hui Min¹, Minwook Kim¹, Youngpil Jeon¹, Minyong Choi¹
Samsung Electronics, [†] Corresponding author
junhong1.min@samsung.com

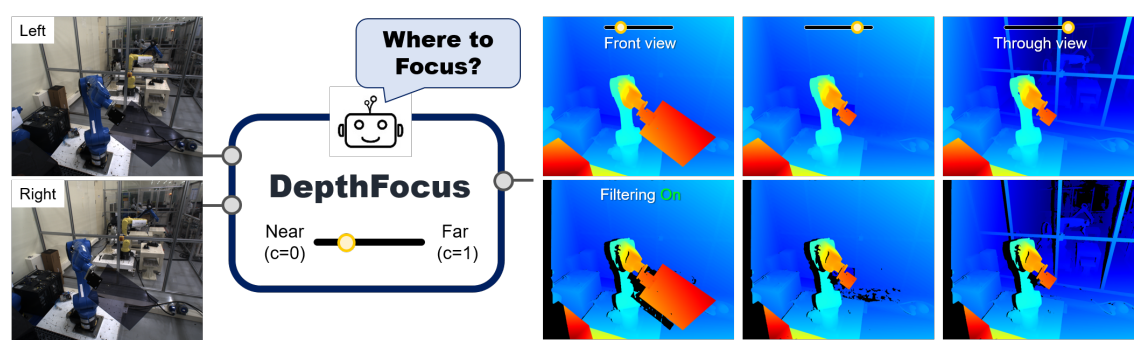


Figure 1. **DepthFocus** resolves depth ambiguity in see-through scenes by allowing users to control the focus range (near–far). Our method generates multiple depth maps based on user preference, which can be fused into a more complete 3D reconstruction.

Abstract

Depth in the real world is rarely singular. Transmissive materials create layered ambiguities that confound conventional perception systems. Existing models remain passive, attempting to estimate static depth maps anchored to the nearest surface, while humans actively shift focus to perceive a desired depth. We introduce DepthFocus, a steerable Vision Transformer that redefines stereo depth estimation as intent-driven control. Conditioned on a scalar depth preference, the model dynamically adapts its computation to focus on the intended depth, enabling selective perception within complex scenes. The training primarily leverages our newly constructed 500k multi-layered synthetic dataset, designed to capture diverse see-through effects. DepthFocus not only achieves state-of-the-art performance on conventional single-depth benchmarks like BOOSTER, a dataset notably rich in transparent and reflective objects, but also quantitatively demonstrates intent-aligned estimation on our newly proposed real and synthetic multi-depth datasets. Moreover, it exhibits strong generalization capabilities on unseen see-through scenes, underscoring its robustness as a significant step toward active and human-like 3D perception.

1. Introduction

Accurate 3D perception is a fundamental prerequisite for intelligent agents, supporting navigation, manipulation, and

scene understanding in robotics and autonomous vehicles. Yet depth is not singular in the real world; multiple depths coexist through transparent or semi-translucent surfaces, forming layered structures that are pervasive in everyday environments. Human vision is not a passive capture of the first visible surface. It actively adapts to context and intent, shifting focus between foreground barriers and background objects as needed. However, in robotics, safety considerations have led to methods that aim to detect the first visible surface to avoid collisions. While effective for immediate safety, these methods inherently fail to capture the full 3D structure of the scene, limiting comprehensive understanding. Moreover, even the seemingly simpler task of estimating the first surface is far from solved. Existing methods often struggle with consistency, producing unreliable results in challenging conditions. Ambiguity is also scale- and context-dependent: a wire fence, solid up close, becomes a see-through medium from a distance, creating profound pixel-level uncertainty. For autonomous agents to achieve human-level interaction, they must be able to reason about 3D structure beyond these complex layers.

Accurate image-based depth estimation has achieved remarkable progress in recent years, with feed-forward models producing results of near-human fidelity across diverse domains. Monocular methods recover fine-grained details with accurate metric scale [3, 4, 16, 20, 50, 51], while videobased approaches ensure temporal consistency across long sequences [7, 17, 43]. Stereo matching provides robust

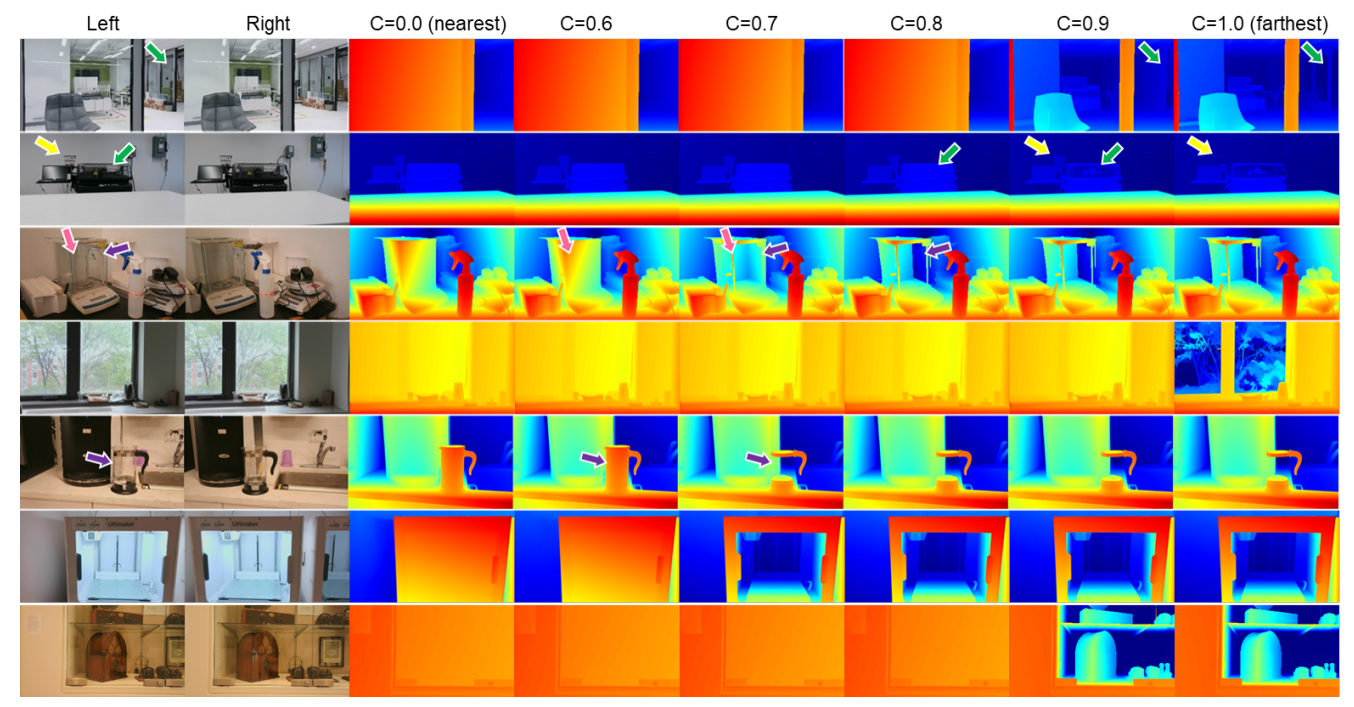


Figure 2. Strong generalization on the LayeredFlow dataset [45] demonstrates that **DepthFocus** effectively handles multi-layered depth environments. By adapting to user intent, our model aligns depth in transmissive regions and adjusts layers according to distance control c.

generalization and precise metric scale, maintaining accuracy even on challenging non-Lambertian surfaces and textureless regions [2, 8, 13, 18, 32, 42, 44]. More recently, unified feed-forward models jointly infer globally consistent poses and dense geometry from unconstrained image sets [23, 40, 41, 49, 55]. Despite these advances, existing approaches remain fundamentally passive, producing static depth maps anchored to the nearest surface and leaving multilayered, see-through regions largely unaddressed.

Recognizing this gap, a recent surge of research has begun to tackle multi-layer depth estimation [30, 37, 46]. These studies generally aim for explicit layer-wise regression, predicting multiple depth layers simultaneously, whether focusing on two-layer object-centric scenarios or more complex multi-layer configurations. While technically ambitious, such approaches do not reflect the human strategy of adjusting perception based on intended depth. So far, they have yet to demonstrate sufficient validation across diverse real-world scenes, showing limited performance and failing to generalize reliably.

In this paper, we challenge the passive paradigm of depth estimation by introducing a general framework for intent-driven depth perception. At the core of this framework is the principle that depth estimation should be controllable: the computational pathway adapts to a user-specified depth of interest. This reframing moves beyond approaches that estimate only the nearest surface or recover a fixed set of depth layers. Instead, it treats depth as an active perceptual dimension inspired by human vision, aligning with the

broader notion of active perception [1, 15, 22, 38, 53], in which sensing adapts dynamically to goals and context.

While our framework is general, we instantiate it within stereo vision. Monocular methods lack inherent metric scale, and unconstrained multiview approaches, though broadly applicable, introduce additional ambiguity in estimating camera relationships and recovering accurate scale. Stereo provides well-calibrated multiview input with stable metric scale, enabling us to focus on the core challenge of multi-layered depth ambiguity. Within this stereo instantiation, we design a novel steerable Vision Transformer architecture equipped with conditional modules. A single, continuous scalar representing the user's depth of interest guides these modules, operating through both direct condition injection and conditional Mixture-of-Experts routing. This enables feature processing to adapt dynamically to the intended depth condition.

To train the model, we internally constructed a large-scale synthetic multi-layer dataset that provides supervision for intent-driven depth perception. For evaluation, we release two complementary resources: (i) a synthetic test set with diverse scenes and see-through materials, covering multi-layered depth under controlled conditions, and (ii) a laboratory-level bilayer real dataset with dense ground-truth annotations, enabling reliable assessment of multi-layer perception. Together, these datasets support comprehensive evaluation in both controlled and real-world environments.

Our experiments demonstrate that the proposed model maintains state-of-the-art performance on conventional

single-depth benchmarks while showing clear improvements in transparent and reflective scenes. On synthetic multi-layered data, it further demonstrates controllable depth estimation aligned with user intent, validating the feasibility of intent-driven perception. Moreover, qualitative results on the LayeredFlow benchmark [45] highlight robust generalization to previously unseen multi-layered scenes (Figure 2).

Our contributions are summarized as follows:

- Intent-driven depth estimation enabling user-controlled focus in multi-layered scenes.
- A steerable Vision Transformer with conditional modules.
- New evaluation resources: a synthetic multi-layered test set and a bilayer real dataset with dense annotations.
- State-of-the-art accuracy on conventional benchmarks and robust generalization to see-through and multi-layered scenes.

2. Related Work

Depth Estimation from Images

Estimating depth from images is a fundamental problem in computer vision. While inherently ill-posed from a single image, recent advances along two complementary axes have significantly improved performance and generalization. Large-scale vision-transformer training has substantially advanced monocular depth prediction by enhancing contextual modeling and enabling transfer across diverse scenes [3, 4, 16, 50]. Meanwhile, generative approaches offer flexible mechanisms to represent uncertainty, generate multiple depth hypotheses, and synthesize plausible metric cues under limited supervision [11, 14, 20]. Extensions to video further emphasize temporal consistency and joint pose–depth estimation [7, 17, 26, 43].

With many unconstrained views, correspondence-based N-view systems learn dense matches and jointly recover globally consistent poses and geometry. For example, DUSt3R employs transformers to learn pixel-level correspondences between arbitrary pairs, bypassing classical SfM initialization [23, 40, 41, 49, 55]. While flexible, these approaches often lack the metric scale necessary for precise measurements. In contrast, stereo methods leverage calibrated pairs and have advanced significantly beyond early CNN-based cost aggregation [6, 21]. A dominant paradigm is iterative cost volume refinement [24, 29, 42, 47], while global matching utilizes Transformers for long-range correspondence [25, 32]. Another trend focuses on robustness in ill-posed regions, such as by incorporating pre-trained monocular depth models as priors [2, 8, 13, 18, 44] or enforcing temporal consistency in video stereo [19]. Despite these advances across monocular, multi-view, and stereo paradigms, they all assume a single consistent depth per pixel, limiting their ability to represent transparent or reflective scenes where multiple surfaces co-exist.

Transparency and Multi-Layer Depth Estimation

The assumption of a single depth value per pixel breaks down in the presence of transparent or reflective surfaces. Early research has primarily focused on recovering the first visible surface or refining noisy sensor measurements through normal prediction, segmentation, or sensor fusion [10, 34, 56]. More recent work explicitly addresses multi-layer ambiguity: stereo-based approaches estimate both the foremost and background depths simultaneously by maintaining parallel disparity hypotheses [30, 37], while monocular methods attempt to reconstruct multiple layers from a single image by predicting several hypotheses or depth distributions per pixel [46]. Similar challenges arise in optical flow, where transparent and reflective regions induce multiple motion layers; benchmarks such as LayeredFlow [45] provide stereocaptured real sequences with sparse multi-layer annotations to study these effects. Collectively, these studies illustrate complementary directions: robust recovery of the first visible surface on the one hand, and reconstruction of all coexisting layers on the other. However, evaluations remain concentrated on synthetic or constrained settings, and precise metric-scale multi-layer reconstruction in diverse real-world environments remains an open challenge.

Conditioned Depth Estimation

Conditioned approaches address depth ambiguity by incorporating external signals as anchors. WorDepth leverages textual priors from pre-trained vision—language models to guide monocular networks toward metric-consistent predictions [54]. DepthLM extends this idea by conditioning a VLM on sparse visual prompts with intrinsic-aware augmentation to normalize focal-length variation, enabling metric queries such as "How far is this point from the camera?" [5]. These methods primarily aim to resolve the scale ambiguity in monocular depth estimation, showing that semantic, visual, or intrinsic cues can provide effective anchors.

3. Method

3.1. Conditional Depth Estimation Framework

We begin by formulating a general framework for conditional depth estimation. Let f(x,c) denote a function that takes an image or image set x and a scalar conditioning variable $c \in [c_0,c_1]$, and outputs a depth map over the image domain. The conditioning variable c is interpreted as a distance preference, enabling controllable estimation across both opaque and transmissive regions without explicit layer indexing.

For a pixel (u,v), let $\mathcal{Z}_{u,v} = \{z_1,z_2,\ldots,z_n\}$ be the set of plausible depths, ordered as $z_1 < z_2 < \cdots < z_n$. The ideal conditional estimator $f_{\text{ideal}}(x,c)$ satisfies:

Property 1: Opaque Determinism. For $(u, v) \in \mathcal{S}_o$, there

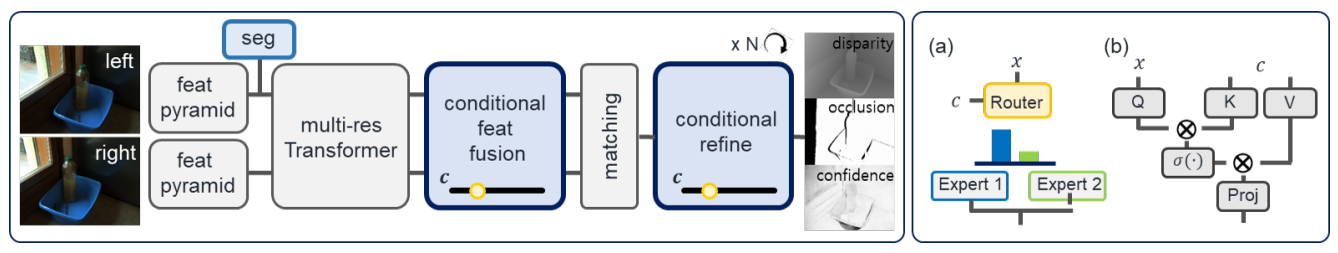


Figure 3. Overview of **DepthFocus** architecture. The model builds on a multi-resolution transformer backbone for global stereo matching, augmented with conditional modules that enable controllable depth adjustment. The right panel illustrates our two conditional operation modules.

exists a unique depth $z_{u,v}$ such that

$$f_{\text{ideal}}(x,c)_{u,v} = z_{u,v}, \quad \forall c \in [c_0, c_1].$$
 (1)

Depth in opaque regions is fixed and independent of c.

Property 2: Monotonicity in Transmissive Regions. For $(u, v) \in \mathcal{S}_t$ and $c_a < c_b$,

$$f_{\text{ideal}}(x, c_a)_{u,v} \le f_{\text{ideal}}(x, c_b)_{u,v}.$$
 (2)

Increasing c consistently shifts the estimate toward farther depths.

Property 3: Distance-Conditioned Diversity. For $(u, v) \in \mathcal{S}_t$, varying c should traverse the plausible set $\mathcal{Z}_{u,v}$:

$$\{f_{\text{ideal}}(x,c)_{u,v} \mid c \in [c_0,c_1]\} \subseteq \mathcal{Z}_{u,v}. \tag{3}$$

Thus c acts as a steerable parameter that selects among valid depths.

In summary, the framework defines depth estimation as a controllable process: opaque regions yield a single fixed depth, while transmissive regions respond to c by revealing alternative plausible surfaces. We next describe conditional modules that instantiate this formulation within a stereo-based matching model.

3.2. Conditional Feature Modulation

To realize the conditional framework in practice, we introduce feature modulation modules that adapt computation according to c. Given an input feature x and conditioning variable c, the following mechanisms adjust feature processing in a condition-aware manner.

(1) Conditional Routing via MoE. Standard FFNs are replaced with conditional Mixture-of-Experts (MoE) layers. A routing network R(x,c) produces weights for combining expert sub-networks $\{E_i\}$:

$$F(x,c) = \sum_{i=1}^{N} R(x,c)_{i} \cdot E_{i}(x).$$
 (4)

Feature processing thus varies with \boldsymbol{c} through weighted expert contributions.

(2) Direct Condition Injection. We also inject c directly into features using a single-item attention block:

$$A(x,c) = \sigma(q_x \cdot k_c) \cdot v_c, \tag{5}$$

where σ is a sigmoid function, q_x is derived from x, and (k_c, v_c) are learned projections of c. The result A(x, c) is added to the feature stream for fine-grained modulation.

Together, routing and injection provide complementary mechanisms to condition feature computation on c, allowing the stereo matching model to realize the properties of the conditional depth estimation framework.

3.3. Conditional Stereo Matching Implementation

Our model builds upon the S2M2 backbone [32], a stateof-the-art stereo framework distinguished by strong multiresolution feature extraction and global matching performance. We adopt S²M² as our baseline and extend it with conditional modules to enable controllable depth estimation. Figure 3 provides an overview of the proposed DepthFocus architecture, illustrating how the multi-resolution backbone is augmented with the two conditional modules introduced in Section 3.2. This design preserves the original pipeline of feature extraction, multi-resolution fusion, and refinement, while embedding conditional operations that make the stereo matching process responsive to the conditioning variable c. Conditional Multi-Resolution Fusion. During coarse-tofine fusion, standard FFN blocks are replaced with conditional modules (MoE routing and direct injection, illustrated in the right panel of Figure 3). At each resolution level, the conditioning variable c modulates the fusion pathway, allowing the network to adaptively emphasize different depth

Conditional Refinement. In the iterative refinement stage, we follow the U-Net structure of S^2M^2 but augment the encoder blocks with the same conditional modules. This ensures that both global propagation and local residual updates remain steerable by c, aligning the final disparity correction with the conditional framework.

layers or surface types.

Segmentation Auxiliary. To improve sim-to-real generalization, we attach lightweight segmentation heads to the FPN output. This heads are trained on monocular segmenta-

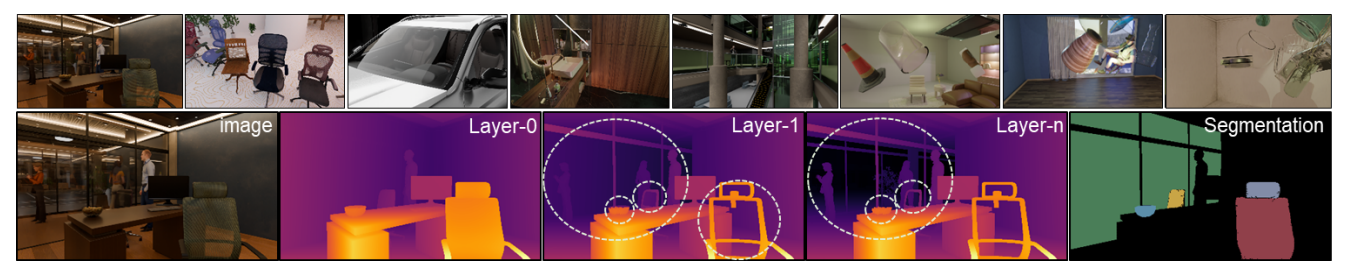


Figure 4. Our multi-layered synthetic dataset. Top row: diverse environments with generated multi-layered depth. Bottom row: annotations capturing depth ambiguities from transmissive and reflective materials.

tion datasets to predict binary masks for reflective and seethrough regions. Although its predictions are not fed back into the stereo pipeline, the auxiliary supervision encourages the backbone to better recognize ambiguous regions, thereby reducing the sim-to-real gap.

3.4. Training with Condition-Aware Supervision

Our training builds on the S²M² framework [32], incorporating condition-aware supervision. The model outputs f(x,c), where $c \in [0,1]$ specifies depth preference. For each c, we define a reference stereo disparity

$$d_{\text{ref}} = (1 - c) \cdot d_{\text{max}},$$

and supervise using the ground-truth depth closest to $d_{\rm ref}$. This yields a single target per pixel, enabling conventional training while adapting to user intent.

To enforce coherence, we introduce a layer-consistency masking strategy that ensures supervision remains structurally aligned across objects and regions. Instead of allowing pixel-wise selections to diverge within the same instance, we identify the dominant layer, the one most consistently represented within a local region, and restrict supervision to its pixels. This approach prevents fragmented training signals, encourages instance-level consistency, and guides the network toward perceptually meaningful depth organization. Prior works such as DIP [39] and DIIP [9] demonstrate that deep networks tend to reconstruct low-dimensional, interpretable structures first, supporting our assumption that layer-aligned supervision can guide perceptually consistent depth selection.

Finally, we add an auxiliary segmentation head trained on monocular data to predict reflectivity and transparency masks. Although not used in stereo inference, this auxiliary task improves sim-to-real generalization by guiding the backbone to better handle ambiguous regions.

4. Dataset Construction

A key challenge in intent-driven depth estimation is the lack of suitable data for training and evaluation. To address this, we introduce a large-scale synthetic dataset and a complementary real-world benchmark, enabling systematic study of multi-layer depth estimation.

4.1. Synthetic Data Generation

We constructed approximately 500k stereo pairs using a procedural pipeline in Blender with diverse transmissive and opaque materials. Scenes were varied in geometry, material properties, and camera parameters to ensure broad coverage of multi-depth ambiguities. Each rendering includes aligned RGB images, per-layer depth, disparity, and segmentation masks. In total, 3,577 scene configurations were generated (see Figure 4). Further details of the generation pipeline are provided in the supplementary material.

4.2. Test Benchmark Dataset

4.2.1. Synthetic Test Set

Our synthetic test set comprises five representative scenes: bedroom, office, cafe, gallery, and outdoor. These cover both indoor and outdoor environments. Each scene contains 85–140 frames, for a total of 535 frames at 2448×2048 resolution. Objects include windows, tables, display cases, cups, vases, lamps, eyewear, and mesh chairs, providing diverse depth ambiguities.

4.2.2. Real-World Multi-Layer Test Set

For real-world evaluation, we collected five scenes using acrylic plates with two levels of transmissivity (60% and 80%). A robotic arm positioned the plates between the stereo sensor and the scene to create two-depth configurations. The transmitted depths were annotated by removing the plate and scanning the scene with a high-precision structured-light 3D scanner. For each scene, we varied both camera viewpoint and plate placement to obtain 12 configurations. Together with the three plate conditions (no plate, 80%, and 60%), this yields $3\times5\times12=180$ stereo pairs, forming our real-world multi-layer benchmark.

5. Experiments

5.1. Implementation

We utilize a base model (channel 192, 1 block) for ablations and a larger model (channel 384, 2 blocks) for benchmarks, both featuring a two-expert conditional MoE module. Training was conducted on H100 GPUs at 768×512 resolution (batch size 8, 1M iterations), followed by 100k iterations of multi-resolution fine-tuning. Our training data combines

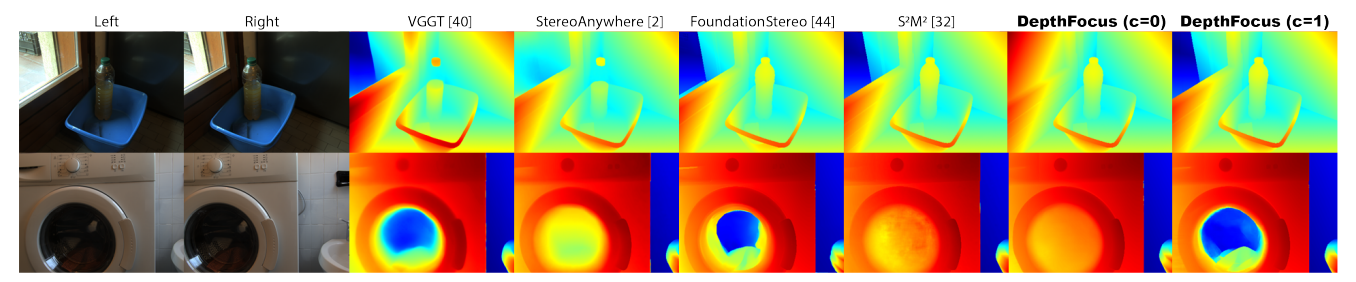


Figure 5. Comparison on the Booster dataset [33], which contains many transmissive/reflective regions. **DepthFocus** provides accurate front-surface and reliable through-view results, while other methods yield inconsistent predictions.



Figure 6. Sample scenes from our real test dataset with varying transmissivity: (a) no plate, (b) 80% transmissivity, and (c) 60% transmissivity.

2M public single-disparity stereo pairs [32] and 500k synthetic multi-layered pairs. We apply a curation strategy to the single-disparity data, broadly categorizing transmissive regions into near-surface and background layers. This coarse categorization enables partial condition-aware supervision despite inconsistent annotations, while our synthetic dataset provides explicit multi-layer supervision. During training, the intent parameter $c \in [0, 1]$ is randomly sampled using a mixed strategy: about half of the samples draw c corresponding to the relative distance between the multi-layered surfaces, while the rest are uniformly sampled in [0, 1]. Finally, we used existing glass/mirror datasets [12, 27, 28, 48] augmented with our custom 5k images for an auxiliary segmentation loss. Further details on dataset construction, augmentation, curation, expert specialization, gating, and training dynamics are provided in the Supplementary Material.

5.2. Results on Existing Single Depth Benchmarks

We first evaluate DepthFocus on standard single-depth stereo benchmarks using conventional metrics, including End-Point Error (EPE) and Bad-x error rates. While our main goal is controllable depth adjustment in multi-layered scenarios, it is essential to verify competitiveness in traditional first-surface estimation. For this, we set the model to nearest-depth prediction.

BOOSTER Benchmark [33]

The BOOSTER benchmark provides fine-grained annotations, enabling comparisons across opaque regions and highly reflective/transmissive regions. As shown in Table 1, DepthFocus achieves state-of-the-art results, with a clear margin in these challenging cases. We compare against our baseline model S²M²-(ft) [32], which is fine-tuned with

the same synthetic dataset. Even with identical training data, DepthFocus achieves superior performance thanks to its controllable depth adjustment design, offering a more effective way to handle reflective and transmissive scenarios. Models using the DA-v2 prior [50] diverge in performance: StereoAnywhere [2] performs well, while FoundationStereo [44] struggles, underscoring the importance of prior integration. We also include VGGT [40] in qualitative analysis (Figure 5); it is omitted from quantitative results as it lacks consistent metric scale and qualitatively fails on these regions.

Middlebury [35] & ETH3D Benchmarks [36]

We evaluate DepthFocus on the representative Middlebury (v3) [35] and ETH3D [36] benchmarks. Middlebury provides high-resolution color images, whereas ETH3D consists of low-resolution grayscale data. Both datasets contain only rare transmissive or reflective regions, yet they remain challenging due to complex scene structures, textureless areas, and strong specular reflections. As shown in Table 2, DepthFocus ranks second on most metrics by a very small margin, closely trailing our baseline model S²M² [32]. This demonstrates that although our approach is designed for controllable depth adjustment in multi-layered scenarios, it remains highly competitive on traditional benchmarks with minimal transparency or reflection content.

5.3. Evaluation on Multi-Layer Depth Estimation

Having established strong performance on conventional single-layer stereo benchmarks (Sec. 5.2), we now focus on our main contribution: intent-driven multi-layer depth estimation. We evaluate this capability through three complementary experiments.

Our Synthetic Benchmark

We quantitatively evaluate DepthFocus under two user-controlled settings, c=0 (first surface) and c=1 (last surface). Results show that our model maintains high accuracy in opaque regions while faithfully reconstructing the intended layer in transmissive regions. Although performance on the last surface is lower due to scattering, attenuation, and internal reflections that obscure deeper layers, the model

		Non-Occlusion							All Pixels						
Model	All		Opaque		Refl/Trans		All		Opaque		Refl/Trans				
	EPE	Bad-4	EPE	Bad-4	EPE	Bad-4	EPE	Bad-4	EPE	Bad-4	EPE	Bad-4			
RAFTStereo [29]	7.11	21.79	3.67	15.93	14.30	48.25	7.56	23.32	4.42	20.42	14.92	48.81			
CREStereo [24]	4.71	14.75	2.66	6.95	17.16	49.95	5.10	16.09	3.09	11.08	18.94	50.41			
PCVNet [52]	5.89	13.34	1.91	7.72	20.27	37.12	6.21	14.91	2.49	11.95	20.96	37.78			
StereoAnywhere [2]	2.77	14.21	1.97	9.73	6.49	39.82	3.03	15.46	2.29	11.96	6.78	40.18			
FoundationStereo [44]	7.20	10.28	1.94	6.91	34.78	53.37	7.52	11.56	2.66	9.94	36.33	53.74			
S ² M ² -(ft) [32]	2.53	8.53	1.89	4.43	7.69	25.52	2.94	9.67	2.13	14.29	9.59	26.17			
DepthFocus (c=0)	2.34	7.53	1.78	6.49	3.88	18.82	2.47	8.73	1.89	7.30	4.08	19.65			

Table 1. Quantitative results on the **BOOSTER** benchmark [33], which contains a large proportion of transmissive and reflective regions. Bold indicates the best score, and underlined numbers mark the second-best score.

			ET			Middlebury v3							
Model	Non-Occ				All			Non-Occ			All		
	EPE	Bad-1	Bad-2	EPE	Bad-1	Bad-2	EPE	Bad-2	Bad-4	EPE	Bad-2	Bad-4	
CREStereo [24]	0.13	0.98	0.22	0.14	1.09	0.29	1.15	3.71	2.04	2.10	8.13	5.05	
Sel-IGEV [42]	0.12	1.23	0.22	0.15	1.56	0.51	0.91	2.51	1.36	1.54	6.04	3.74	
CAS [31]	0.14	0.87	0.32	0.15	1.09	0.21	1.01	3.33	1.77	1.52	6.29	3.75	
BridgeDepth [13]	0.10	0.38	0.11	0.11	0.50	0.16	0.78	3.78	1.61	1.48	6.92	3.48	
FoundationStereo [44]	0.09	0.26	0.08	0.13	0.48	0.26	0.78	1.84	1.04	1.24	4.26	2.72	
S ² M ² [32]	0.10	0.22	0.06	0.10	0.26	0.08	0.69	1.15	0.54	1.00	2.94	1.63	
DepthFocus (c=0)	0.10	0.25	0.07	0.10	0.29	0.09	0.74	1.53	0.83	1.08	3.63	2.13	

Table 2. Quantitative results on the **ETH3D** [36] and **Middlebury v3** [35] stereo benchmarks. For ETH3D, metrics include EPE, Bad-1, and Bad-2. For Middlebury, metrics include EPE, Bad-2, and Bad-4. Both Non-Occlusion and All-Pixels regions are reported. Bold indicates the best score, and underlined numbers mark the second-best score.

		Opaque				Transmissive								
Model	-					First				Last				
Model	EPE	Bad-1	Bad-2	Bad-4	EPE	Bad-1	Bad-2	Bad-4	EPE	Bad-1	Bad-2	Bad-4		
Sel-IGEV [42]	3.00	11.60	7.87	5.52	32.40	80.20	72.75	63.02	-	-	-	-		
StereoAnywhere [2]	4.32	27.80	17.76	12.45	16.63	75.17	62.47	49.68	-	-	-	-		
FoundationStereo [44]	0.78	5.53	3.45	2.10	21.64	58.14	48.97	40.04	-	-	-	-		
S ² M ² [32]	0.79	5.19	3.19	2.06	6.30	27.74	19.86	14.23	-	-	-	-		
S ² M ² -(ft) [32]	0.72	5.14	3.09	1.96	3.06	17.38	10.90	7.45	-	-	-	-		
DepthFocus (c=0)	0.70	4.60	2.90	1.90	2.15	14.83	8.53	5.42	39.14	93.40	88.06	79.46		
DepthFocus (c=1)	0.73	4.66	2.93	1.95	41.03	92.71	87.43	79.15	6.59	40.56	31.07	22.68		

Table 3. Quantitative results on **our synthetic benchmark**. We report performance on opaque regions and transmissive regions, where **DepthFocus** is evaluated with user-controlled settings c=0 (first surface) and c=1 (last surface). Existing methods are evaluated only the first layer as intended by design. Bold indicates the best score, and uanderlined numbers mark the second-best score.

Model	No Plate		Plate (Tr	ansmittance	Plate (Transmittance 80%)						
	Opaque	Opaque	Transmissive				Opaque	Transmissive			
	-	-	First		Last		- First		rst	Last	
	Bad-4	Bad-4	Bad-4	Bad-8	Bad-4	Bad-8	Bad-4	Bad-4	Bad-8	Bad-4	Bad-8
StereoAnywhere [2]	5.43	5.39	100.0	99.99	-	-	5.28	99.99	99.99	-	-
FoundationStereo [44]	2.05	2.93	99.90	99.87	-	-	3.60	99.74	99.68	-	-
S ² M ² -(ft) [32]	1.65	2.47	99.13	98.90	-	-	2.92	99.74	99.72	-	-
DepthFocus (c=0)	1.51	3.17	4.72	4.08	96.57	96.31	3.59	74.13	72.65	35.90	34.52
DepthFocus (c=1)	1.52	1.20	99.49	99.29	9.21	7.03	2.01	99.69	99.65	4.11	3.00

Table 4. Quantitative results on **our real benchmark**. We report performance on opaque regions and transmissive regions, where **DepthFocus** is evaluated with user-controlled settings c=0 (first surface) and c=1 (last surface). Existing methods are evaluated only the first layer as intended by design. Bold indicates the best score, and underlined numbers mark the second-best score.

consistently adapts to user intent and recovers the correct layer when possible. In contrast, the StereoAnywhere model fine-tuned on the BOOSTER dataset underperforms on our synthetic benchmark, and FoundationStereo fails to recover the first surface in transmissive regions. Both rely on monocular depth priors, which in practice provide little benefit for resolving multi-layer ambiguity. Moreover, fine-tuning the baseline S²M² on our multi-depth dataset yields limited

gains in opaque regions but significantly improves recovery of the first surface in transmissive areas, highlighting the importance of intent-driven training for multi-layer depth estimation.

Our Controlled Real Benchmark

We next evaluate on laboratory scenes containing transmissive acrylic plates. These scenes present a significant chal-

		Opa	que		Transmissive					
Ablation	C	=0	C	=1	First	(C=0)	Last (C=1)			
Abiation	Bad-2	Bad-4	Bad-2	Bad-4	Bad-2	Bad-4	Bad-2	Bad-4		
Full Model	3.76	2.47	3.75	2.46	12.20	7.63	40.02	29.73		
(-) C-MoE	4.07 (+0.31)	2.68 (+0.21)	4.21 (+0.46)	2.75 (+0.29)	16.43 (+4.23)	11.22 (+3.59)	41.86 (+1.84)	32.33 (+2.60)		
(-) DCI	4.19 (+0.43)	2.70 (+0.23)	4.31 (+0.56)	2.81 (+0.35)	16.19 (+3.99)	10.52 (+2.89)	42.06 (+2.04)	31.51 (+1.78)		
(-) Seg Loss	4.17 (+0.41)	2.73 (+0.26)	4.30 (+0.55)	2.85 (+0.39)	13.10 (+0.90)	8.69 (+1.06)	38.93 (-1.09)	28.70 (-1.03)		
(-) Data Curation	4.50 (+0.74)	2.93 (+0.46)	4.71 (+0.96)	3.11 (+0.65)	15.24 (+3.04)	10.18 (+2.55)	41.23 (+1.21)	32.10 (+2.37)		

Table 5. Ablation study on our synthetic benchmark. We report performance on opaque regions and transmissive regions (First / Last). Each row corresponds to the full model or the model with one component removed. Here, **C-MoE** is the Conditional Mixture-of-Experts module, **DCI** the Direct Condition Injection module, **Seg Loss** the auxiliary segmentation loss with syn/real datasets, and **Data Curation** the strategy for leveraging the existing single-disparity datasets.

lenge due to the unfamiliar setting and the absence of semantic cues, such as window frames, around the "floating" plates. In the absence of transmissive plates, most existing algorithms exhibit performance trends comparable to those observed on conventional single-depth benchmarks. However, when plates are present, baselines heavily relying on monocular priors, such as StereoAnywhere [2] and FoundationStereo [44], consistently fail to recover the first surface. This indicates that monocular structural cues are ineffective in this challenging environment lacking contextual information. In contrast, DepthFocus successfully resolves the two-layer ambiguity for plates with 60% transmissivity. It demonstrates controllable recovery of both the foremost and transmitted depths. For plates with 80% transmissivity, however, our model struggles to detect the front layer. This performance drop highlights the intrinsic difficulty of such extreme cases where even human perception struggles due to the severe lack of semantic context compared to the training distribution.

Qualitative Evaluation on Real Benchmark [45]

Finally, we qualitatively evaluate DepthFocus on real-world transmissive scenes using the LayeredFlow benchmark [45], which contains diverse multi-depth environments with complex materials and illumination. Despite training primarily on synthetic multi-layer data, DepthFocus handles objects and optical properties not seen during training, including variations in geometry, surface finish, and reflectance. As shown in Figure 2, our method follows user control and progressively reveals scene structures across depths. Real transmissive scenes often contain more than two overlapping layers, and our model produces stable, interpretable transitions even in such three-layer cases. These results demonstrate that DepthFocus effectively manages complex real-world scenarios while supporting flexible, intention-driven reconstruction.

5.4. Ablation Study

We analyze the impact of each component in Table 5. Both conditional modules prove effective in controlling multi-layer depths, particularly in transmissive regions where depth ambiguity is severe. The Conditional Mixture-of-Experts

(C-MoE) yields slightly higher gains compared to Direct Condition Injection (DCI). Regarding the auxiliary segmentation loss, we observe a slight performance difference in the synthetic benchmark. We attribute this to the identical distribution of training and testing data in our synthetic setup. However, we retain this loss because it helps improve generalization in unseen real-world environments, as shown in the Supplementary Material. In contrast, removing our data curation strategy causes significant degradation across all regions. This confirms that effectively leveraging the large-scale single-disparity dataset is essential, indicating that data scale remains a critical factor for overall performance.

6. Discussion

While our method generalizes well, a few representative limitations remain. One key challenge arises when reflection and transmission layers exhibit similar intensities, making them difficult to separate using single-view cues, which can lead to misinterpretation of reflected structures as valid scene geometry, particularly in complex see-through materials. Another limitation occurs when layers are very closely spaced, as subtle distance changes may not be sufficient to fully distinguish them. It is worth noting that even humans may struggle to resolve multiple overlapping transmissive layers under similar conditions, highlighting the inherent difficulty of the task. Addressing these issues through explicit modeling of reflected depth, analogous to our treatment of transmissive layers, and incorporating temporal information could provide complementary cues for more reliable disambiguation.

7. Conclusion

We propose a generalized conditional approach for resolving multi-depth ambiguities, implemented within a stereo matching framework. By steering predictions according to the intended distance, our method effectively disentangles complex scene layers. Extensive experiments demonstrate both quantitative and qualitative effectiveness, validating the model across diverse see-through scenarios. Ultimately, this work establishes intent-driven depth control as a practical step toward active 3D perception.

References

- [1] Ruzena Bajcsy. Active perception. *Proceedings of the IEEE*, 76(8):966–1005, 1988. 2
- [2] Luca Bartolomei, Fabio Tosi, Matteo Poggi, and Stefano Mattoccia. Stereo anywhere: Robust zero-shot deep stereo matching even where either stereo or mono fail. In *Proceedings of the Computer Vision and Pattern Recognition Conference*, pages 1013–1027, 2025. 2, 3, 6, 7, 8
- [3] Shariq Farooq Bhat, Reiner Birkl, Diana Wofk, Peter Wonka, and Matthias Müller. Zoedepth: Zero-shot transfer by combining relative and metric depth. *arXiv preprint arXiv:2302.12288*, 2023. 1, 3
- [4] Aleksei Bochkovskii, AmaÃĢl Delaunoy, Hugo Germain, Marcel Santos, Yichao Zhou, Stephan R Richter, and Vladlen Koltun. Depth pro: Sharp monocular metric depth in less than a second. arXiv preprint arXiv:2410.02073, 2024. 1, 3
- [5] Zhipeng Cai, Ching-Feng Yeh, Hu Xu, Zhuang Liu, Gregory Meyer, Xinjie Lei, Changsheng Zhao, Shang-Wen Li, Vikas Chandra, and Yangyang Shi. Depthlm: Metric depth from vision language models. arXiv preprint arXiv:2509.25413, 2025. 3
- [6] Jia-Ren Chang and Yong-Sheng Chen. Pyramid stereo matching network. In Proceedings of the IEEE/CVF Conference on Computer Vision and Pattern Recognition, pages 5410–5418, 2018. 3
- [7] Sili Chen, Hengkai Guo, Shengnan Zhu, Feihu Zhang, Zilong Huang, Jiashi Feng, and Bingyi Kang. Video depth anything: Consistent depth estimation for super-long videos. In *Proceedings of the Computer Vision and Pattern Recognition Conference*, pages 22831–22840, 2025. 1, 3
- [8] Junda Cheng, Longliang Liu, Gangwei Xu, Xianqi Wang, Zhaoxing Zhang, Yong Deng, Jinliang Zang, Yurui Chen, Zhipeng Cai, and Xin Yang. Monster: Marry monodepth to stereo unleashes power. In *Proceedings of the Computer Vision and Pattern Recognition Conference*, pages 6273–6282, 2025. 2, 3
- [9] Hamadi Chihaoui and Paolo Favaro. Diffusion image prior. In Proceedings of the IEEE/CVF International Conference on Computer Vision (ICCV), pages 24636–24644. Computer Vision Foundation, 2025. Open Access version. 5
- [10] Alex Costanzino, Pierluigi Zama Ramirez, Matteo Poggi, Fabio Tosi, Stefano Mattoccia, and Luigi Di Stefano. Learning depth estimation for transparent and mirror surfaces. In Proceedings of the IEEE/CVF International Conference on Computer Vision, pages 9244–9255, 2023. 3
- [11] Xiao Fu, Wei Yin, Mu Hu, Kaixuan Wang, Yuexin Ma, Ping Tan, Shaojie Shen, Dahua Lin, and Xiaoxiao Long. Geowizard: Unleashing the diffusion priors for 3d geometry estimation from a single image. In *European Conference on Computer Vision*, pages 241–258. Springer, 2024. 3
- [12] Mark Edward M. Gonzales, Lorene C. Uy, and Joel P. Ilao. Designing a lightweight edge-guided convolutional neural network for segmenting mirrors and reflective surfaces. *Computer Science Research Notes*, 3301:107–116, 2023. 6
- [13] Tongfan Guan, Jiaxin Guo, Chen Wang, and Yun-Hui Liu. Bridgedepth: Bridging monocular and stereo reasoning with

- latent alignment. In *Proceedings of the IEEE/CVF International Conference on Computer Vision*, pages 27681–27691, 2025. 2, 3, 7
- [14] Ming Gui, Johannes Schusterbauer, Ulrich Prestel, Pingchuan Ma, Dmytro Kotovenko, Olga Grebenkova, Stefan Andreas Baumann, Vincent Tao Hu, and Björn Ommer. Depthfm: Fast generative monocular depth estimation with flow matching. In Proceedings of the AAAI Conference on Artificial Intelligence, pages 3203–3211, 2025. 3
- [15] Charles Herrmann, Richard Strong Bowen, Neal Wadhwa, Rahul Garg, Qiurui He, Jonathan T Barron, and Ramin Zabih. Learning to autofocus. In *Proceedings of the IEEE/CVF Conference on Computer Vision and Pattern Recognition*, pages 2230–2239, 2020. 2
- [16] Mu Hu, Wei Yin, Chi Zhang, Zhipeng Cai, Xiaoxiao Long, Hao Chen, Kaixuan Wang, Gang Yu, Chunhua Shen, and Shaojie Shen. Metric3d v2: A versatile monocular geometric foundation model for zero-shot metric depth and surface normal estimation. *IEEE Transactions on Pattern Analysis and Machine Intelligence*, 2024. 1, 3
- [17] Wenbo Hu, Xiangjun Gao, Xiaoyu Li, Sijie Zhao, Xiaodong Cun, Yong Zhang, Long Quan, and Ying Shan. Depthcrafter: Generating consistent long depth sequences for open-world videos. In *Proceedings of the Computer Vision and Pattern Recognition Conference*, pages 2005–2015, 2025. 1, 3
- [18] Hualie Jiang, Zhiqiang Lou, Laiyan Ding, Rui Xu, Minglang Tan, Wenjie Jiang, and Rui Huang. Defom-stereo: Depth foundation model based stereo matching. In *Proceedings of* the Computer Vision and Pattern Recognition Conference, pages 21857–21867, 2025. 2, 3
- [19] Junpeng Jing, Weixun Luo, Ye Mao, and Krystian Mikolajczyk. Stereo any video: Temporally consistent stereo matching. Proceedings of the IEEE international conference on computer vision, 2025. 3
- [20] Bingxin Ke, Anton Obukhov, Shengyu Huang, Nando Metzger, Rodrigo Caye Daudt, and Konrad Schindler. Repurposing diffusion-based image generators for monocular depth estimation. In *Proceedings of the IEEE/CVF conference on computer vision and pattern recognition*, pages 9492–9502, 2024. 1, 3
- [21] Alex Kendall, Hayk Martirosyan, Saumitro Dasgupta, Peter Henry, Ryan Kennedy, Abraham Bachrach, and Adam Bry. End-to-end learning of geometry and context for deep stereo regression. In *Proceedings of the IEEE international conference on computer vision*, pages 66–75, 2017. 3
- [22] Justin Kerr, Kush Hari, Ethan Weber, Chung Min Kim, Brent Yi, Tyler Bonnen, Ken Goldberg, and Angjoo Kanazawa. Eye, robot: Learning to look to act with a bc-rl perception-action loop. arXiv preprint arXiv:2506.10968, 2025.
- [23] Vincent Leroy, Yohann Cabon, and Jérôme Revaud. Grounding image matching in 3d with mast3r. In *European Conference on Computer Vision*, pages 71–91. Springer, 2024. 2, 3
- [24] Jiankun Li, Peisen Wang, Pengfei Xiong, Tao Cai, Ziwei Yan, Lei Yang, Jiangyu Liu, Haoqiang Fan, and Shuaicheng Liu. Practical stereo matching via cascaded recurrent network with adaptive correlation. In *Proceedings of the IEEE/CVF*

- Conference on Computer Vision and Pattern Recognition, pages 16263–16272, 2022. 3, 7
- [25] Zhaoshuo Li, Xingtong Liu, Nathan Drenkow, Andy Ding, Francis X Creighton, Russell H Taylor, and Mathias Unberath. Revisiting stereo depth estimation from a sequenceto-sequence perspective with transformers. In *Proceedings of* the IEEE/CVF International Conference on Computer Vision, pages 6197–6206, 2021. 3
- [26] Zhengqi Li, Richard Tucker, Forrester Cole, Qianqian Wang, Linyi Jin, Vickie Ye, Angjoo Kanazawa, Aleksander Holynski, and Noah Snavely. MegaSaM: Accurate, fast and robust structure and motion from casual dynamic videos. arXiv preprint, 2024. 3
- [27] Jiaying Lin, Yuen Hei Yeung, and Rynson WH Lau. Exploiting semantic relations for glass surface detection. In *Proc. NeurIPS*, 2022. 6
- [28] Jiaying Lin, Xin Tan, and Rynson WH Lau. Learning to detect mirrors from videos via dual correspondences. In *Proceedings* of the IEEE/CVF conference on computer vision and pattern recognition, pages 9109–9118, 2023. 6
- [29] Lahav Lipson, Zachary Teed, and Jia Deng. Raft-stereo: Multilevel recurrent field transforms for stereo matching. In *International Conference on 3D Vision (3DV)*, pages 218–227. IEEE, 2021. 3, 7
- [30] Zhidan Liu, Chengtang Yao, Jiaxi Zeng, Yuwei Wu, and Yunde Jia. Multi-label stereo matching for transparent scene depth estimation. arXiv preprint arXiv:2505.14008, 2025. 2, 3
- [31] Junhong Min and Youngpil Jeon. Confidence aware stereo matching for realistic cluttered scenario. In 2024 IEEE International Conference on Image Processing (ICIP), pages 3491–3497. IEEE, 2024. 7
- [32] Junhong Min, Youngpil Jeon, Jimin Kim, and Minyong Choi. S²M²: Scalable stereo matching model for reliable depth estimation. *arXiv preprint arXiv:2507.13229*, 2025. 2, 3, 4, 5, 6, 7
- [33] Pierluigi Zama Ramirez, Fabio Tosi, Matteo Poggi, Samuele Salti, Stefano Mattoccia, and Luigi Di Stefano. Open challenges in deep stereo: the booster dataset. In *Proceedings of* the IEEE/CVF Conference on Computer Vision and Pattern Recognition, pages 21168–21178, 2022. 6, 7
- [34] Shreeyak Sajjan, Matthew Moore, Mike Pan, Ganesh Nagaraja, Johnny Lee, Andy Zeng, and Shuran Song. Clear grasp: 3d shape estimation of transparent objects for manipulation. In 2020 IEEE international conference on robotics and automation (ICRA), pages 3634–3642. IEEE, 2020. 3
- [35] Daniel Scharstein, Heiko Hirschmüller, York Kitajima, Greg Krathwohl, Nera Nešić, Xi Wang, and Porter Westling. High-resolution stereo datasets with subpixel-accurate ground truth. In Pattern Recognition: 36th German Conference, GCPR 2014, Münster, Germany, September 2-5, 2014, Proceedings 36, pages 31–42. Springer, 2014. 6, 7
- [36] Thomas Schops, Johannes L Schonberger, Silvano Galliani, Torsten Sattler, Konrad Schindler, Marc Pollefeys, and Andreas Geiger. A multi-view stereo benchmark with high-resolution images and multi-camera videos. In *Proceedings of the IEEE/CVF Conference on Computer Vision and Pattern Recognition*, pages 3260–3269, 2017. 6, 7

- [37] Jun Shi, A Yong, Yixiang Jin, Dingzhe Li, Haoyu Niu, Zhezhu Jin, and He Wang. Asgrasp: Generalizable transparent object reconstruction and 6-dof grasp detection from rgb-d active stereo camera. In 2024 IEEE international conference on robotics and automation (ICRA), pages 5441–5447. IEEE, 2024. 2, 3
- [38] Kevin J Shih, Saurabh Singh, and Derek Hoiem. Where to look: Focus regions for visual question answering. In *Proceedings of the IEEE conference on computer vision and pattern recognition*, pages 4613–4621, 2016. 2
- [39] Dmitry Ulyanov, Andrea Vedaldi, and Victor Lempitsky. Deep image prior. In Proceedings of the IEEE conference on computer vision and pattern recognition, pages 9446–9454, 2018. 5
- [40] Jianyuan Wang, Minghao Chen, Nikita Karaev, Andrea Vedaldi, Christian Rupprecht, and David Novotny. Vggt: Visual geometry grounded transformer. In *Proceedings of the Computer Vision and Pattern Recognition Conference*, pages 5294–5306, 2025. 2, 3, 6
- [41] Shuzhe Wang, Vincent Leroy, Yohann Cabon, Boris Chidlovskii, and Jerome Revaud. Dust3r: Geometric 3d vision made easy. In Proceedings of the IEEE/CVF Conference on Computer Vision and Pattern Recognition, pages 20697–20709, 2024. 2, 3
- [42] Xianqi Wang, Gangwei Xu, Hao Jia, and Xin Yang. Selectivestereo: Adaptive frequency information selection for stereo matching. In *Proceedings of the IEEE/CVF Conference* on Computer Vision and Pattern Recognition, pages 19701– 19710, 2024. 2, 3, 7
- [43] Jamie Watson, Oisin Mac Aodha, Victor Prisacariu, Gabriel Brostow, and Michael Firman. The temporal opportunist: Self-supervised multi-frame monocular depth. In *Proceedings of the IEEE/CVF conference on computer vision and pattern recognition*, pages 1164–1174, 2021. 1, 3
- [44] Bowen Wen, Matthew Trepte, Joseph Aribido, Jan Kautz, Orazio Gallo, and Stan Birchfield. Foundationstereo: Zeroshot stereo matching. In *Proceedings of the Computer Vision and Pattern Recognition Conference*, pages 5249–5260, 2025. 2, 3, 6, 7, 8
- [45] Hongyu Wen, Erich Liang, and Jia Deng. Layeredflow: A real-world benchmark for non-lambertian multi-layer optical flow. In *European Conference on Computer Vision*, pages 477–495. Springer, 2024. 2, 3, 8
- [46] Hongyu Wen, Yiming Zuo, Venkat Subramanian, Patrick Chen, and Jia Deng. Seeing and seeing through the glass: Real and synthetic data for multi-layer depth estimation. *arXiv* preprint arXiv:2503.11633, 2025. 2, 3
- [47] Gangwei Xu, Yun Wang, Junda Cheng, Jinhui Tang, and Xin Yang. Accurate and efficient stereo matching via attention concatenation volume. *IEEE Transactions on Pattern Analysis and Machine Intelligence*, 46(4):2461–2474, 2023. 3
- [48] Mingchen Xu, Peter Herbert, Yu-Kun Lai, Ze Ji, and Jing Wu. Rgb-d video mirror detection. In 2025 IEEE/CVF Winter Conference on Applications of Computer Vision (WACV), pages 9640–9649. IEEE, 2025. 6
- [49] Jianing Yang, Alexander Sax, Kevin J Liang, Mikael Henaff, Hao Tang, Ang Cao, Joyce Chai, Franziska Meier, and Matt

- Feiszli. Fast3r: Towards 3d reconstruction of 1000+ images in one forward pass. In *Proceedings of the Computer Vision and Pattern Recognition Conference*, pages 21924–21935, 2025. 2. 3
- [50] Lihe Yang, Bingyi Kang, Zilong Huang, Zhen Zhao, Xiao-gang Xu, Jiashi Feng, and Hengshuang Zhao. Depth anything v2. Advances in Neural Information Processing Systems, 37: 21875–21911, 2024. 1, 3, 6
- [51] Wei Yin, Jianming Zhang, Oliver Wang, Simon Niklaus, Long Mai, Simon Chen, and Chunhua Shen. Learning to recover 3d scene shape from a single image. In *Proceedings of the IEEE/CVF conference on computer vision and pattern recog*nition, pages 204–213, 2021. 1
- [52] Jiaxi Zeng, Chengtang Yao, Lidong Yu, Yuwei Wu, and Yunde Jia. Parameterized cost volume for stereo matching. In Proceedings of the IEEE/CVF International Conference on Computer Vision, pages 18347–18357, 2023. 7
- [53] Rui Zeng, Yuhui Wen, Wang Zhao, and Yong-Jin Liu. View planning in robot active vision: A survey of systems, algorithms, and applications. *Computational Visual Media*, 6(3): 225–245, 2020. 2
- [54] Ziyao Zeng, Daniel Wang, Fengyu Yang, Hyoungseob Park, Stefano Soatto, Dong Lao, and Alex Wong. Wordepth: Variational language prior for monocular depth estimation. In Proceedings of the IEEE/CVF Conference on Computer Vision and Pattern Recognition, pages 9708–9719, 2024.
- [55] Junyi Zhang, Charles Herrmann, Junhwa Hur, Varun Jampani, Trevor Darrell, Forrester Cole, Deqing Sun, and Ming-Hsuan Yang. Monst3r: A simple approach for estimating geometry in the presence of motion. In *ICLR*, 2025. 2, 3
- [56] Luyang Zhu, Arsalan Mousavian, Yu Xiang, Hammad Mazhar, Jozef van Eenbergen, Shoubhik Debnath, and Dieter Fox. Rgb-d local implicit function for depth completion of transparent objects. In *Proceedings of the IEEE/CVF Con*ference on Computer Vision and Pattern Recognition, pages 4649–4658, 2021. 3